DEVELOPMENT OF POROSITY OF CEMENT PASTE BLENDED WITH SUPPLEMENTARY CEMENTITIOUS MATERIALS AFTER CARBONATION

Wu B[1*], Ye G[2, 3]
[1, 2] *Microlab, Delft University of Technology, 2628 CN, Delft, The Netherlands*
[3] *Magnel Laboratory for Concrete Research, Ghent University, 9052 Ghent, Belgium*

Abstract: Supplementary cementitious materials (SCMs) like fly ash (FA) and blast furnace slag (BFS) are normally used to replace parts of Ordinary Portland cement (OPC) to reduce the cost and CO_2 emission. Some consequences are the reduction of portlandite (CH) content and the formation of C-S-H with low Ca/Si ratio, due to pozzolanic reactions. It is known that carbonation of portlandite leads to a reduction in the porosity which is ascribed to the positive difference of molar volumes between CH and $CaCO_3$. However, the influence on the porosity caused by the carbonation of C-S-H is still controversial. The molar volume change due to the carbonation of C-S-H depends on the properties of C-S-H (like Ca/Si ratio, water content) and the water remained in silica gel. Moreover, the decalcification of C-S-H with the Ca/Si ratio lower than 1.2 can cause more structure changes and shrinkage of C-S-H. During the carbonation of cement paste blended with SCMs, less portlandite but a relatively high amount of C-S-H with low Ca/Si ratio will be carbonated. The pore structure will evolve in a different way, comparing with Portland cement paste. Therefore, it's very important to figure out the pore structure development of cement paste blended with SCMs under carbonation.

In this paper, the binary cement pastes (B70, blended with blast furnace slag, and F30, blended with fly ash) and ternary cement pastes (F10B54 and F30B30, blended with blast furnace slag and fly ash) are studied and compared with Portland cement paste. Mercury Intrusion Porosimetry (MIP) and nitrogen adsorption isotherm are used to determine the pore volume and size distribution of capillary pores and gel pores (2-37 nm), respectively. Thermogravimetric analysis (TGA) is used to determine the amounts of portlandite and $CaCO_3$. The results show that the amount profiles of portlandite and $CaCO_3$ can be used as a more accurate method to study the carbonation in blended cement paste, comparing with the phenolphthalein test. Carbonation of most of the species of C-S-H results in the increase of the porosity of cement paste. $CaCO_3$ contributed by the carbonation of low Ca C-S-H is dominant in blended cement paste B70, F10B54 and F30B30. Both the total and effective capillary porosity increases in the above-mentioned paste after the carbonation. Moreover, total porosities of B70 and F10B54 increase with the increasing amount of C-S-H involving in carbonation. However, the increment of the total porosity of F30B30 decreases with the increasing amount of C-S-H being carbonated. Carbonation of C-S-H increases the volume and size of the small gel pore, and creates more capillary pores. This peculiar phenomenon is more evident for the mixture with a higher proportion of SCMs, like B70 and F30B30. The results reveal that the carbonation of C-S-H formed in pozzolanic reactions cause the increase of the total and capillary porosity in cement paste blended with SCMs, which will bring adverse effects on the durability of blended cement concrete exposed to the carbonation.

Originality
Carbonation profiles (porosity, contents of CH and $CaCO_3$) are drawn for cement paste blended with SCMs, including binary and ternary system, after accelerated carbonation. Carbonation of C-S-H in blended cement paste contributes the increase of the porosity, which is confirmed in this study. The increases of total and effective capillary porosity are also observed in the carbonated cement paste blended with a relatively high amount of SCMs, such as B70, F10B54 and F30B30. The relationship is established between the porosity of blended cement paste and the amount of C-S-H being carbonated. The structure evolution of C-S-H during carbonation is illustrated on the basis of the colloid C-S-H model; the corresponding changes to the gel pore structure are interpreted as well.
Keywords: porosity, pore volume distribution, SCMs, cement paste, accelerated carbonation

[1] **Corresponding author: B.Wu@tudelft.nl, Tel +31-15-2781492, Fax +31-15-276383**

1. Introduction

Carbonation of calcium-bearing phases inside the concrete is the main deterioration process of infrastructure in open district with high average annual relative humidity. The consequence of this ageing phenomenon is the reduction of alkalinity, which makes the reinforcement easy to be corroded. In general, calcium-bearing phases involving in carbonation could be hydration products like portlandite (CH), calcium silicate hydrate (C-S-H) , as well as unhydrated cement clinkers like tricalcium silicate (C_3S), dicalcium silicate(C_2S). Normally, the reactions between unhydrated cement and CO_2 can be ignored because their weak competition for CO_2 in front of CH and C-S-H (Peter, Muntean et al. 2008). From thermodynamic point of view, the carbonation of CH has a priority comparing with C-S-H (Glasser and Matschei 2007). However in experiments the initial rate of carbonation is quite similar (Morandeau, Thiery et al. 2014). Therefore, the main carbonation reactions happened inside the concrete are as follows:

$$CH + \overline{C} \rightarrow C\overline{C} + H \quad (1)$$

$$C_xSH_y + x\overline{C} \rightarrow xC\overline{C} + SH_t + (y-t)H \quad (2)$$

It is reclaim that, in cement notations, $C = CaO$, $H = H_2O$, $S = SiO_2$, $A = Al_2O_3$, and $\overline{C} = CO_2$. x, y and t are the molecular numbers. As the number of S is normally set as one when describing the formula of C-S-H, x and y also equal to the Ca/Si and H_2O/Si ratio.

It is universally acknowledged that the carbonation of CH leads to a reduction in porosity which is ascribed to the positive difference of molar volume between CH and the formed $CaCO_3$ (Pihlajavaara 1968, Pihlajavaara and Pihlman 1974, Patel, Killoh et al. 1988, Papadakis, Vayenas et al. 1991, Ngala and Page 1997, Delmi, Aı¨t-Mokhtar et al. 2006). But if considering the carbonation of C-S-H, the effect of the carbonation on the porosity and microstructure of cement paste is still controversial. Carbonation of C-S-H has been studied by many authors (Zdeneˇk Sˇauman 1972, Black, Breen et al. 2007, Morandeau, Thiery et al. 2014). It agreed that a complex decalcification-polymerization process of the C-S-H and the formation of amorphous silica gel, see equation (2). The molar volume change due to the carbonation of C-S-H depends on the properties of C-S-H (like Ca/Si ratio, water content) and the water remained in silica gel.

In Portland cement paste, the Ca/Si ratio (C/S) in C-S-H is about 1.5-1.9. The addition of supplementary cementitious materials (SCMs) like fly ash results in the formation of a C-S-H with lower C/S, which is generally agreed to have a tobermorite- like structure $C_{0.83}S_2H_{1.5}$ but with many defects, mainly in bridging tetrahedron (Cong and Kirkpatrick 1996, Cong and Kirkpatrick 1996, Richardson 1999). The formation of C-S-H with a low C/S leads to an increased uptake of aluminium in the C-S-H, called C-A-S-H (Richardson and Groves 1993). Therefore, in cement paste blended with SCMs like fly ash, there are at least two types of C-S-H: C-S-H with high C/S from the hydration of C_3S and C_2S (high Ca C-S-H), C-S-H with low C/S from the pozzolanic reaction (low Ca C-(A-) S-H). The proportions of them are determined by the replacement level of SCMs, which is confirmed by the thermodynamic modelling from B. Lothenbach et al (Lothenbach, Scrivener et al. 2011). Moreover, the decalcification of C-S-H may cause the shrinkage of cement paste, especially for the C-S-H with Ca/Si lower than 1.2 (Chen, Thomas et al. 2006).

In cement paste blended with SCMs, the amount of CH is quite lower than that in the Portland cement paste. More proportion of C-S-H with high or low Ca/Si ratio is carbonated. The changes of microstructure due to carbonation is mainly caused by the carbonation of C-S-H, or the complex mixture which consists of different types of C-S-H. Therefore, concerning the influence of carbonation on the microstructure of SCMs blended cement paste, the limited data which were published in the scientific literature do not show a real consensus.

The aim of this work is to provide further evidence and improved understanding of the effects of carbonation on the microstructure (porosity and pore size distribution) of cement paste blended with different SCMs, on the basis of mercury intrusion porosimetry and nitrogen adsorption isotherm. By correlating the investigations of microstructure with the

measurements of the phases evolving in the carbonation performed by thermogravimetric analysis, the carbonation profiles (porosity, contents of CH and $C\overline{C}$) are provided, in order to obtain reliable analytical relations representing the behavior of cement paste blended with different kinds of SCMs exposed to the carbonation, including ternary mixture.

2. Experimental

2.1. Raw Materials

Ordinary Portland cement (PC) used in the study was type CEM I 425N, from ENCI in the Netherlands. Fly ash (FA) and blast furnace slag (BFS) were used to replace part of PC in cement paste blended with SCMs. FA is Class F fly ash, according to ASTM C 618. BFS is produced by ECOCEM in the Netherlands. Main chemical compositions of raw materials are determined by X-ray fluorescence spectrometry (XRF). The results are compared in table 1.

Major crystalline phases of above raw materials were tested by X-ray diffraction (XRD). The X-ray source used is Cu K radiation (λ = 0.154056 nm). The scan step size was 0.03°, from 5° to 70° (2θ). X-ray test results are shown in Figure 1.

Table 1 Main chemical composition of raw materials by XRF (wt. %)

	CaO	SiO_2	Al_2O_3	Fe_2O_3	MgO	K_2O	Na_2O	SO_3	L.O.L	CO_2[a]
Cement	66.15	18.34	4.41	3.46	2.16	0.46	-	2.63	1.37	0.80
FA	5.61	49.79	31.81	5.38	1.05	0.90	0.18	0.49	2.35	0.11
BFS	39.86	34.85	11.90	0.47	9.78	0.29	-	1.69	0.1	0.0

[a] *Calculated from TGA*

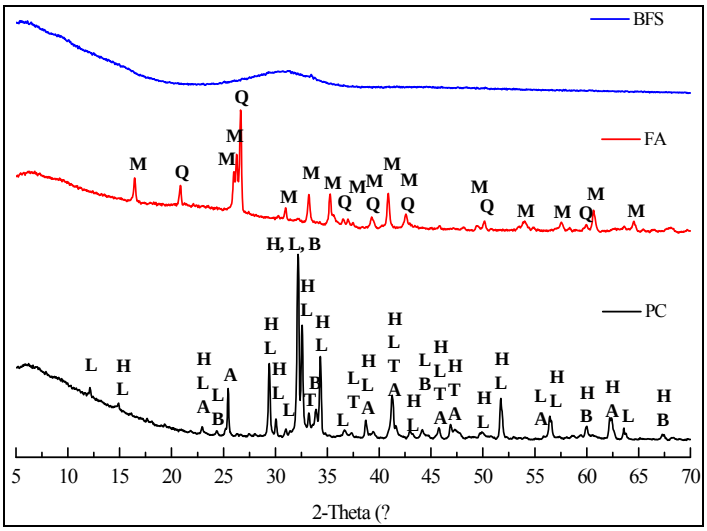

Figure 1 X- ray diffraction analysis of the raw materials

Based on the X-ray test result, the major mineral composition of Portland cement clinker was determined by Rietveld method[1]. If unidentified or amorphous phases exist in the mixture, the refinement by Rietveld method will results in overestimated weight percentage. Therefore, a standard powder with a known crystal structure and amount was mixed with the samples as the internal standard. In this research, corundum (Al_2O_3, PDF #74-1081) was used as the internal standard; the percentage of corundum was approximate 10% of the total weight. The mineralogical composition of the used raw materials determined by XRD Rietveld are listed in table 2.

Table 2 Major crystalline composition of Portland cement clinker and FA determined by Retiveld method (wt. %)

	OPC clinker		FA	BFS
Alite (Hatrurite, Ca_3SiO_5)	54.6	Quartz (SiO_2)	10.6	
Belite (Larnite, Ca_2SiO_4)	29.0	Mullite ($Al_{4.8}O_{9.6}Si_{1.2}$)	19.2	
Aluminate ($Ca_3Al_2O_6$)	6.16	Amorphous	70.2	100
Ferrite (Ca_2AlFeO_5)	6.83			
Sulfate (Anhydrite, $CaSO_4$)	0.56			
Lime (CaO)	2.35			

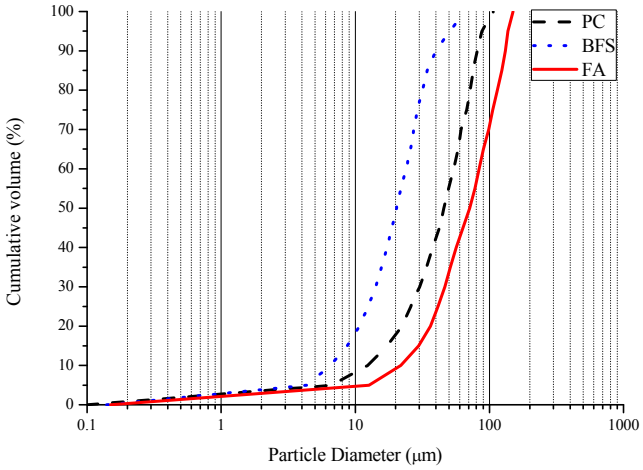

Figure 2 Particle size distribution of raw materials (dash ---- PC, solid — FA, dot •••• BFS)

The particle size distributions of raw materials analyzed by Laser Diffraction are shown in Figure 2.

2.2. Sample preparation and experimental procedure

Pure Portland cement paste was prepared as the blank sample. In blended cement paste, PC was partially replaced by FA or BFS, including binary (PC + FA or BFS) and ternary system (PC + FA + BFS). The mixture design is given in table 3. All the materials are in weight percentage with respect to total binder content. The water/binder ratio (W/B) is 0.5. Different cement pastes were prepared in a HOBART mixer under the room temperature. The binders were mixed with demineralized water at the low speed for 1 minute and at the high speed for 2 minutes with interval pause for 15 seconds. The fresh paste was transferred immediately to the plastic bottles with the diameter of 50 mm. The bottles were filled in 3 steps and vibrated for 10 seconds at each step to remove the air before the bottles were sealed. Then, those bottles were fixed in the rotation machine at a speed of 5-7 rpm for 24 hours to prevent bleeding. Sealed curing was performed for all specimens at 20 °C in the fog room for 12 months before carbonation test.

After curing, plastic bottles were cut into two pieces in order to obtain two cylinders (height = 40 mm, φ =50 mm, as shown in Figure 3a). Both top face rims and bottom face of part B were re-sealed with silicon sealant in order to obtain unidimensional carbonation condition. Then the samples were moved into the carbonation chamber regulated by CO_2 concentration of 3%±0.2, at 20 °C and 75% of relative humidity (using the saturated NaCl solution). The carbonation ages were up to 84 days.

After carbonation for the certain date, plastic cover and silicon sealant of cylinder samples were removed and cleaned. The samples were cut into two half-cylinders in the middle. The fresh cutting surface were sprayed with phenolphthalein to measure the carbonation depth. Then slices were sawn from the two half-cylinders of the same sample, step by step from the exposed surface to the deeper inside area of the sample. Thickness of the slice was approximate 2 mm. The schematic graph for cutting the slice is described in Figure 3b.

Slices of cement pastes were immersed into liquid nitrogen for 3-4 min to stop the further hydration. Then these specimens were immediately moved into a vacuum freeze-dryer. The temperature and vacuum were maintained at -24 °C and 0.1 Pa, respectively(Ye 2003). The drying procedure would last for at least 4 weeks until the daily weight loss of those specimens was lower than 0.1%. Then the specimens were ready for the following tests.

Table 3 Mass fraction of raw materials in different mixtures

Sample ID	PC (g) (wt. %)	FA (g) (wt. %)	BFS (g) (wt. %)	H_2O (g)
P100	1500			750
F30	1050	450 (30)		750
B70	450		1050 (70)	750
F10B54	540	150 (10)	810 (54)	750
F30B30	600	450 (30)	450 (30)	750

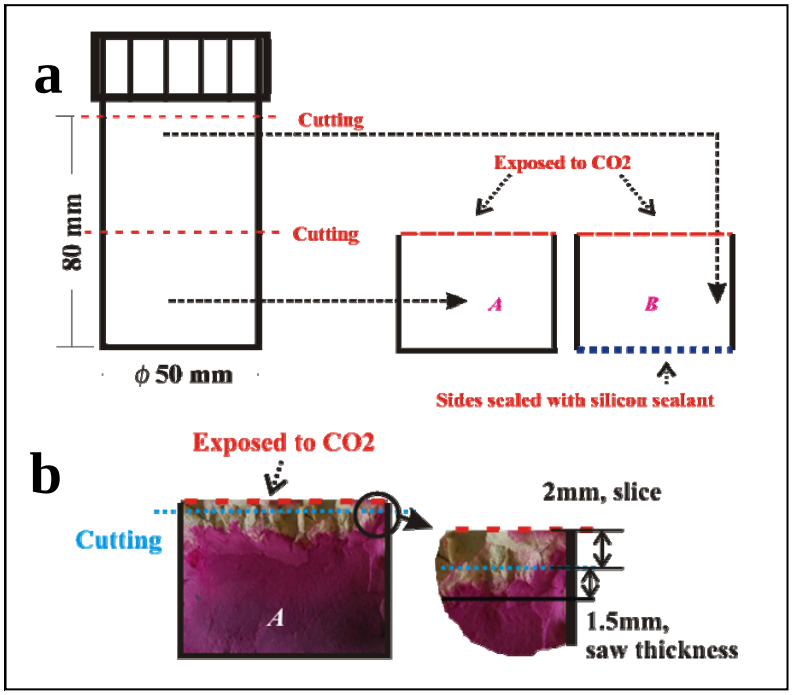

Figure 3 Sample pretreatment before the accelerate carbonation test

2.3. Test methodology

2.3.1 Mercury Intrusion Porosimetry (MIP)

In the MIP measurement the maximum pressure applied was 207 MPa, which means the effectively measurable pore size was the range of 0.007-500 μm. Each measurement consists of three stages: intrusion at the low pressure running from 0 to 0.170MPa; intrusion at the high pressure running from 0.170 to 205 MPa; following by the extrusion back to 0.170 MPa. Each specimen were tested for 2 or 3 times. The total porosity and effective capillary porosity also can be calculated on the basis of the MIP test results (Ye 2003).

2.3.2 Nitrogen adsorption

The gel pore structure (2-37 nm) was measured by nitrogen adsorption isotherm, which is a method for estimating the pore volume and area distribution calculated by the BJH (Joyner, Barrett et al. 1951). Nitrogen adsorption tests were conducted by using Gemimi VII 2390 with a relative pressure range from 0.05~0.98.

2.3.3 Thermogravimetric analysis (TGA)

Thermogravimetric analysis (TGA) is the method to provide information about the decomposition or dehydration of minerals as a function of temperature. Coupled with a mass spectrometer, more accurate temperature range for the decomposition of CH and C-S-H can be obtained. The contents of main hydration products (CH and C-S-H) were calculated from the weight loss of samples from TGA curves. The well-dried samples were ground into powder with an average particle size <75 μm. The mass of powder samples was 30-50 mg. The samples was heated at the rate of 10°C/ min from 40-1100°C. TGA tests were carried out by the Netzsch STA 449 F3 Jupiter coupled with a mass spectrometer (MS) Netzsch QMS 403 C Quadrupole under a dry argon atmosphere, in order to identify with the more accurate temperature range related to the emissions of H_2O and CO_2.

3. Results and Discussion

3.1 Profiles of the portlandite and the amounts of $CaCO_3$

The typical TGA-MS results for cement paste before and after carbonation are shown in Figure 4. By using MS, the ion currents of different gases are recorded, providing gas information during the heating. In the TGA curve of noncarbonated sample, the weight loss in the range of 40-400°C is normally related to the dehydration of C-S-H (Noumowé 1995, Richard 1999), part of the carboaluminate hydrates (Nonnet, Lequeux et al. 1999), AFm and AFt (Zhou and Glasser 2001) phases, as well as to the emission of physically-bound water (Noumowé 1995). This is confirmed by the mass spectrum of H_2O (see Figure 4a). There is a

minor peak around 180°C in the mass spectrum of H_2O and the DTG curve, indicating the presence of monocarbonate (Lothenbach, Le Saout et al. 2008). Coupled with MS results, the mass loss related to CH dehydroxylation usually occurs in the range of 450-550 °C (Noumowé 1995, Platret 2002). Weight loss due to the dehydration of CH is determined by a graphical technique (Marsh and Day 1988). The technique makes a correction for the concurrent dehydration of other compounds.

The decomposition of $CaCO_3$ mainly happens in the range of 600-900 °C (Noumowé 1995, Grattan-Bellew 1996). Considering together with the DTG curve in Figure 4b, the two obvious peaks in CO_2 MS curve are due to the decarbonation of (aragonite) and β-$CaCO_3$ (calcite), respectively. MS patterns confirm that the CO_2 starts to release in the same temperature range as CH. This is due to the presence of amorphous forms of calcium carbonate (Cole and Kroone 1960, Baird, Cairns-Smith et al. 1975, Moorehead 1986, Brečević and Nielsen 1989, Stepkowska, Blanes et al. 2004, Stepkowska, Aviles et al. 2007). Moreover, in the DTG curve of carbonated blended cement paste, there is one more peak at lower temperature, which is not obvious in the DTG curve of carbonated Portland cement paste (Figure 4b). It indicates the decomposition of μ-$CaCO_3$ (vaterite). Both aragonite and vaterite are metastable calcium carbonate forms, and they are in particular formed from the carbonation of C-S-H with low Ca/Si ratio (Black, Breen et al. 2007).

To figure out the proportion of CO_2 released from different kinds of calcium carbonate, the CO_2 mass spectrum is fitted by multi-Gaussian peaks. The decomposition temperature of different kinds of $CaCO_3$ is determined by the fitting result. Then the relative percentage of different types of $CaCO_3$ is calculated from TG curve, which are shown in table 4.

The amount of calcite decreases but the content of other carbonates increases with the increase of SCMs content. The reason is that calcite is mainly formed from the carbonation of portlandite and other carbonates are mainly produced from the carbonation of C-S-H. Comparing with F30, more amorphous $CaCO_3$ but less vaterite and aragonite are formed in B70 after carbonation.

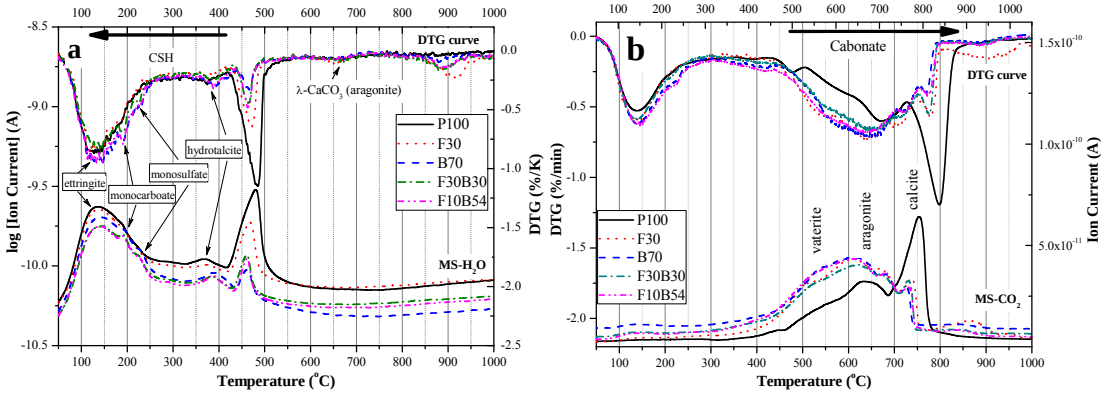

Figure 4 TGA-MS coupled test results of cement paste w/b = 0.5: (a) Hydrated for 1 year; (b) Hydrated for 1 year, then carbonated for 84 days, the outermost surface part with a depth of 2mm.

Table 4 Decomposition temperature and the relative percentage of different calcium carbonate

Mixture	Relative mass percentage of $CaCO_3$ (%)			
	Amorphous $CaCO_3$	Vaterite	Aragonite	Calcite
P100	9.1	19.96	43.45	27.49
	(424-508 °C)	*(510-621 °C)*	*(592-754 °C)*	*(750-806 °C)*
F30	19.95	32.38	40.37	7.29
	(327-609 °C)	*(493-597 °C)*	*(601-754 °C)*	*(760-784 °C)*
B70	29.43	30.56	36.97	3.04
	(394-572 °C)	*(522-626 °C)*	*(622-748 °C)*	*(754-770 °C)*
F30B30	16.39	29.49	50.13	3.99
	(352-504°C)	*(505-619 °C)*	*(615-755 °C)*	*(757-775 °C)*
F10B54	11.81	42.86	41.08	4.26
	(358-452 °C)	*(494-635 °C)*	*(619-750°C)*	*(756-776 °C)*

Due to the decomposition of polymorphs of $CaCO_3$, the quantification method used for CH is less appropriate. However, considering both the MS of CO_2 and DTG curve, the weight loss in the range of 500-825 °C is indicated to the decomposition of $CaCO_3$ and used for the quantification.

According to the decomposition reactions of portlandite and $CaCO_3$,

$$\begin{array}{ccccccc} Ca(OH)_2 & \rightarrow & CaO & + & H_2O & & \\ 74g/mol & & 56g/mol & & 18g/mol & & \\ CaCO_3 & \rightarrow & CaO & + & CO_2 & & \\ 100g/mol & & 56g/mol & & 44g/mol & & \end{array} \quad (3)$$

the portlandite or $CaCO_3$ amount per 1g of freeze-dried cement paste can be calculated by equation 3 and 4, respectively.

$$w_{(CH)} = w_H^{CH} \times \frac{74g/mol}{18g/mol} \qquad w_{(C\bar{C})} = w_C^{C\bar{C}} \times \frac{100g/mol}{44g/mol} \quad (4)$$

Where: w_H^{CH} and $w_C^{C\bar{C}}$ are the weight loss determined by TGA, due to the decomposition of portlandite or $CaCO_3$. The calculated results are compared in Figure 5.

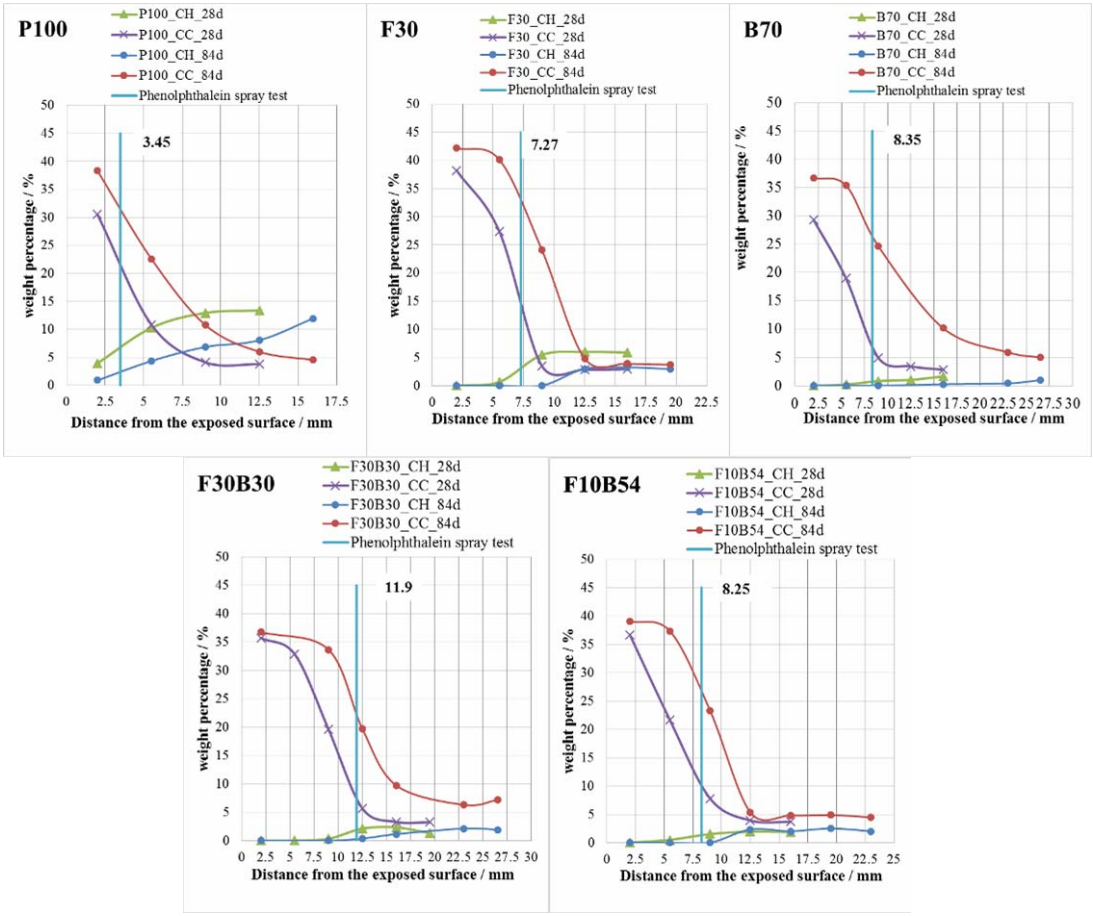

Figure 5 Profiles of the amounts of portlandite and $CaCO_3$ in cement paste after carbonation. (Hydrated for 1 year, then carbonated for 28 and 84 days). The carbonation depth was tested from the samples carbonated for 84 days, using phenolphthalein spray test.

Incorporating SCMs into cement paste causes the reduction of the portlandite content, due to the dilution effect and pozzolanic reaction. Normally, the higher amount of SCMs, the lower amount of portlandite. During the carbonation, the portlandite is converted into $CaCO_3$. Therefore, from the exposed surface to the non-carbonated part, the portlandite content increases from zero, together with the decrease of the $CaCO_3$ amount. Profiles of portlandite and $CaCO_3$ move towards the inside part of the cement paste with the increase of carbonation time. These phase profiles can be used to determine the carbonation front or depth. In the

profiles, the depth, where the amounts of both portlandite and $CaCO_3$ become almost unchanged, is considered as the carbonation depth. The depth determined by this method is compared with that measured by phenolphthalein test in table 5. Carbonation depth determined by TGA-MS shows much higher than that determined by the phenolphthalein. It should be noticed that the increasing amount of $CaCO_3$ with the extension of carbonation time, is mainly contributed by the carbonation of C-S-H in cement paste blended with a high amount of SCMs, such as B70, F10B54 and F30B30.

Table 5 Comparison of carbonation depth tested by two methods

Depth (mm)	P100	F30	B70	F30B30	F10B54
TG	12.5	12.5	22.5	22.5	12.5
phenolphthalein spray	3.45	7.27	8.35	11.9	8.25

3.2 Effects of carbonation on the capillary pore-MIP test results

Pore volume and pore size distribution tested by MIP after carbonation are shown in Figure 6 and Figure 7, in which the test results of binary and ternary mixtures are compared respectively.

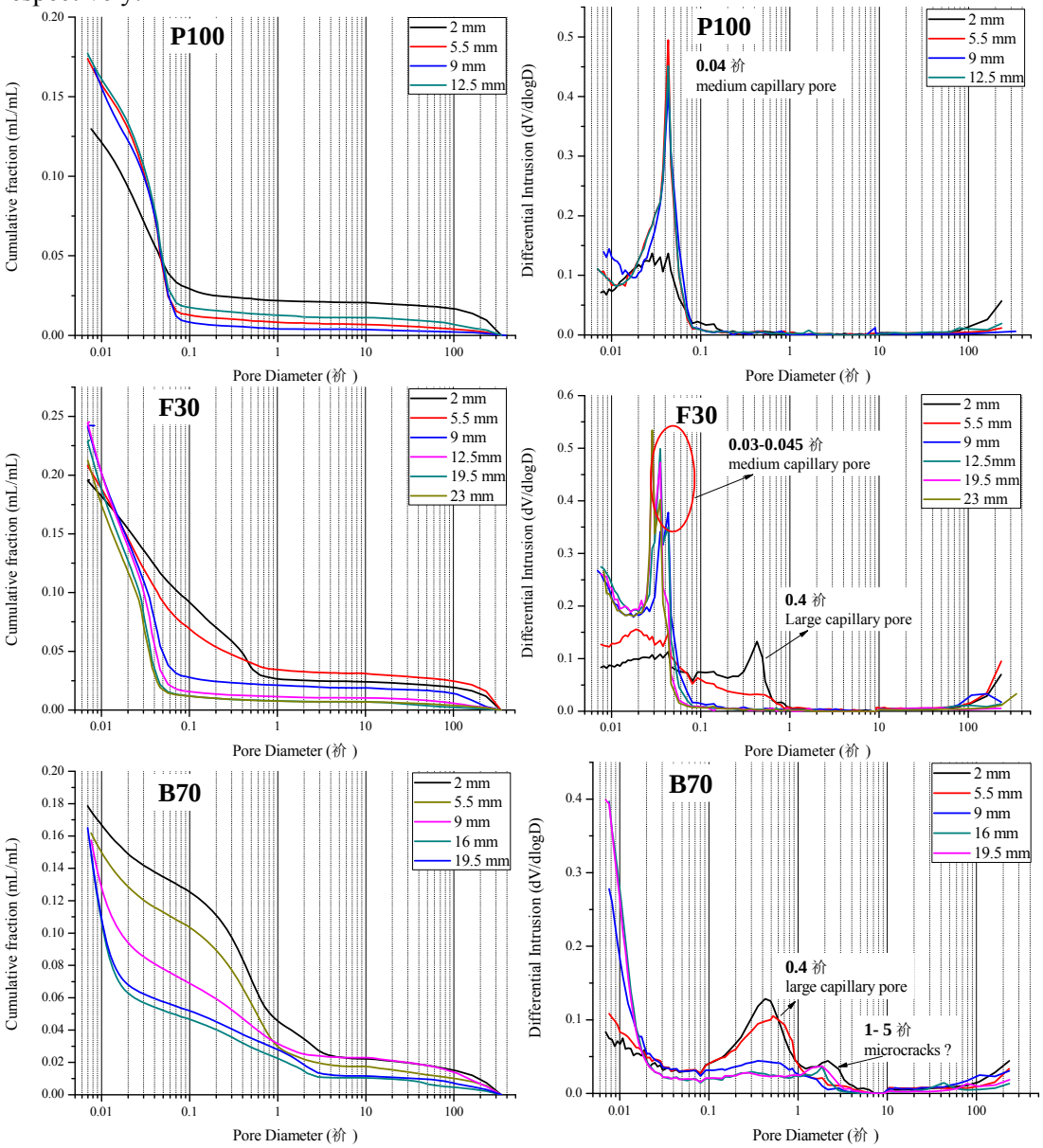

Figure 6 Capillary pore volume and pore size distribution of Portland cement and binary mixture: Portland cement paste (P100), blended with 30% of FA (F30) and blended with 70% of BFS (B70) (Hydrated for 1 year, then carbonated for 84 days).

In general, the pore size distribution differential curve of cement paste measured by MIP, there are two 'critical peak'(Cook and Hover 1999). The first 'critical peak' is in the range of 0.1 to 1 μm, corresponding to large capillary pores; The second 'critical peak' is in the range of 0.01 to 0.1μm, corresponding to medium capillary pores, according to the classification of pores in cement paste by Minders and Young(Mindess, Young et al. 1981). Although the definition of capillary pores is not quite the same in elsewhere (Jennings 2004), the classification and definition by Minders and Young was used in the discussions.

For the Portland cement paste, the pore volume in the range of 0.01-0.1 μm decreases during the carbonation, together with the intensity of the second 'critical peak', which corresponds to the medium capillary pore. The pore volume in the range of 0.1-1.0 μm is approximately the same before and after carbonation. For the noncarbonated part of Portland cement paste, there is no first 'critical peak' in the pore size distribution differential curve.

Normally, carbonation in Portland cement is only responsible for an apparent clogging of the microstructure between 0.01-0.1 μm corresponding to medium capillary pores attributed to the voids among outer C-S-H clusters, which is confirmed by many studies (Pihlajavaara 1968, Matsusato, Ogawa et al. 1992, Puertas, Palacios et al. 2006, Song and Kwon 2007, Auroy, Poyet et al. 2015). This is due to the formation of $C\overline{C}$ in the pores, with a greater molar volume than the initial component CH. However, carbonation is also capable of producing larger capillary pores of 100-200 nm size if W/C or CO_2 concentration is high enough (i.e. W/C > 0.5 or CO_2 > 50%), claimed by some other researchers (Moorehead 1986, Villain and Thiery 2005, Lawrence, Mays et al. 2007, Thiéry, Faure et al. 2011). Chaussadent T et al(Chaussadent, Baroghel-Bouny et al. 2000) studied the relationship between water-cement ratio and hydrate size in cement pastes. Hydrates of a bigger size in porous concretes with higher W/C ratio can be well developed in capillary pores. During the carbonation, the CH dissolves and leaves room to bigger pores and the carbonation products preferably develop in the smaller pores. This is one of the possible reasons for the appearance of pores around 100-200 nm at the same time as the filling of the 30 nm pores. Whatever the effects of carbonation on the capillary pore structure (making it coarser or finer), the total porosity of Portland cement paste (mortar, or concrete) is decreased after the carbonation (natural or accelerated).

For cement paste blended with 30% of FA, the pore volume in the range of 0.02-1 μm, which includes the medium and large capillary pores, increases obviously during carbonation. In the relevant differential curve, there is a shift of the second 'critical peak', corresponding to the medium capillary pore, towards greater pore radii during carbonation, together with the intensity decline. Moreover, the first peak indicating large capillary pores appears, and the intensity of which increases with the carbonation. The creation of coarser capillary pore structure is observed on the carbonated cement paste blended with 30% of FA.

For cement paste blended with 70% of BFS, the pore volume in the range of 0.01-1 μm increases dramatically. There are no critical peaks observed in the differential curve of BFS blended cement paste. However, the peak corresponding to large capillary pores appears during the carbonation. A new 'critical peak' in the range of 1-5 μm, arises after carbonation. It means a much coarser capillary pore structure, comparing with FA blends, is created by the carbonation in B70.

Similar results as B70 can be observed on the ternary mixtures, F10B54 and F30B30 in the pore volume and pore size distribution curves, shown in Figure 7. It should be noticed that the dominated calcium-bearing phase be carbonated is C-S-H in B70, F10B54 and F30B30.

For cement paste (or concrete) blended with FA or BFS, normally the capillary pore volume increases after carbonation, when the amount of FA (> 35%) or BFS (>65%) is high enough (Litvan and Meyer 1986, Ngala and Page 1997, Borges, Costa et al. 2010, Frías and Goñi 2013, Morandeau, Thiéry et al. 2015). This is due to the carbonation of overwhelming amount of C-S-H, especially those with low Ca/Si ratio. The same results can be also observed in this study. But in the above cases, the range of the capillary pore size were not specified. It should be noticed that a 'critical peak' in the range of 1-5μm appears in the differential curves of B70, F10B54 or F30B30 after the carbonation. This is possible due to the microcracks caused by

the carbonation shrinkage. Especially, the carbonation of C-S-H with low Ca/Si ratio (1.2-1.4) can cause relatively more shrinkage of the paste(Chen, Thomas et al. 2006). It means a higher risk of cracking.

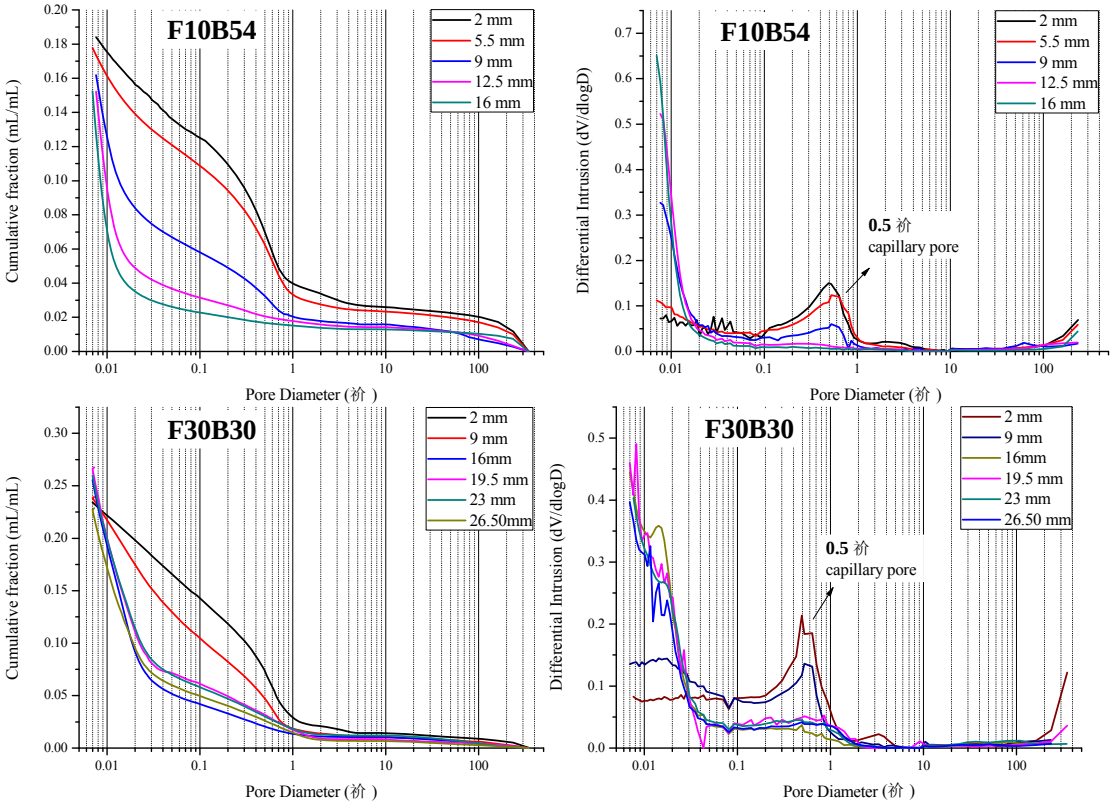

Figure 7 Capillary pore volume and pore size distribution for ternary mixture: cement paste blended with 10% of FA and 54% of BFS (F10B54), blended with 30% of FA and 30% of BFS (F30B30) (hydrated for 1 year, then carbonated for 84 days).

The total porosity and effective capillary porosity are illustrated in Figure 8. Apparently, both the total and effective capillary porosity of Portland cement (P100) and FA blended cement paste (F30) paste decrease after the carbonation. For cement paste blended with a relative higher amount of BFS, like B70, F10B54 and F30B30, the total porosity and effective capillary porosity increase after the carbonation. The same conclusions can be drawn from the tests of concrete under natural carbonation up to 20 years(Litvan and Meyer 1986).

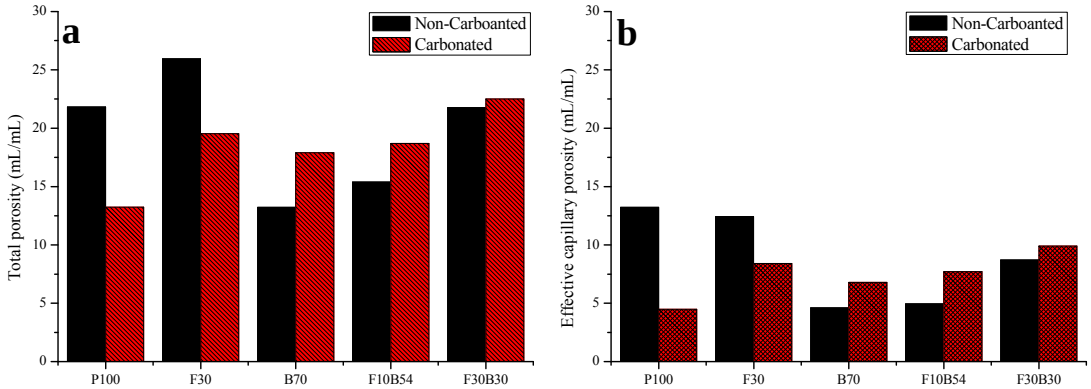

Figure 8 Total porosity (a) and effective capillary porosity (b) of blended cement paste before and after carbonation (hydrated for 1 year, then carbonated for 84 days).

It is known the carbonation of portlandite causes the decline of the porosity. Therefore, the porosity of carbonated cement paste will be lower. However, the porosity of B70 and F10B54 increases after the carbonation. The only reason is that the carbonation of CSH increases the porosity, especially the carbonation of C-S-H with low Ca/Si ratio produced from the pozzolanic reactions.

Based on the equation (1) and (2) describing the carbonations of CH and C-S-H, the solid volume changes due to the carbonation can be expressed as following equation (5) (Morandeau, Thiéry et al. 2015).

$$\phi = \phi_{CH} + \phi_{CSH} = n_{C\bar{C}}^{CH}(V_{C\bar{C}}^{CH} - V_{CH}) + n_{C\bar{C}}^{CSH}[V_{C\bar{C}}^{CSH} + \frac{V_{CSH}(t) - V_{CSH}(t_0)}{C/S(t_0) - C/S(t)}] \quad (5)$$

In which, $V_{C\bar{C}}^{CH} = V_{C\bar{C}}^{CSH} = 36.93\,cm^3/mol$ and $V_{CH} = 3.07 cm^3/mol$, are the molar volume of $C\bar{C}$ and CH respectively. $n_{C\bar{C}}^{CH}$ and $n_{C\bar{C}}^{CSH}$ are the molar number of $C\bar{C}$ contributed by the carbonation of CH and CSH. $C/S(t_0)$ and $C/S(t)$ are the Ca/Si ratio of C-S-H before and after carbonation. $C/S(t_0)$ varies from 0.75-2.0 and $C/S(t)$ equals to zero. $V_{CSH}(t)$ is the molar volume of C-S-H before carbonation; $V_{CSH}(t_0) = V_{SH_t(gel)}$ is the molar volume of carbonation product $SH_t(gel)$, which is in the range of 12-34 cm^3/mol (Thiéry, Faure et al. 2011).

By applying the above-mentioned parameters, the volume change per 1 mole of $C\bar{C}$ contributed by the carbonation of C-S-H can be calculated by equation (6).

$$\phi_{CSH}^0(cm^3/mol) = 36.93 - \frac{V_{CSH}(t_0) - V_{SH_t(gel)}}{C/S(t_0)} \quad (6)$$

The total volume changes due to the carbonation of CH and C-S-H can be calculated by equation (7).

$$\phi = \phi_{CH} + \phi_{CSH} = 3.85 \times n_{C\bar{C}}^{CH} - [36.93 - \frac{V_{CSH}(t_0) - V_{SH_t(gel)}}{C/S(t_0)}] \times n_{C\bar{C}}^{CSH} \quad (7)$$

Making an assumption that $\phi_{CSH}^0 = 0$, then

$$V_{CSH}(t_0) = 36.93 \times C/S(t_0) + V_{SH_t(gel)} \quad (8)$$

The linear relationships between $V_{CSH}(t_0)$ and $C/S(t_0)$ are drawn in Figure 9. The value of $V_{SH_t(gel)}$ is chosen as 12, 20 and 25 cm^3/mol, respectively. The data points in the same figure are the relevant parameters of C-S-H used in the references(Jennings and Tennis 1994, Papadakis 1999, Jennings 2000, Tennis and Jennings 2000, Jennings, Bullard et al. 2008, Lothenbach, Matschei et al. 2008, Thomas, Jennings et al. 2010).

Calculation of volume changes based on the values of the point above the linear curve will give a negative value of $\phi_{CSH}^0(<0)$; otherwise a positive value. The negative value of ϕ_{CSH}^0 means the carbonation of these types of C-S-H will cause a negative increase of the solid volume and the increase of the pore space volume or porosity of the cement paste matrix.

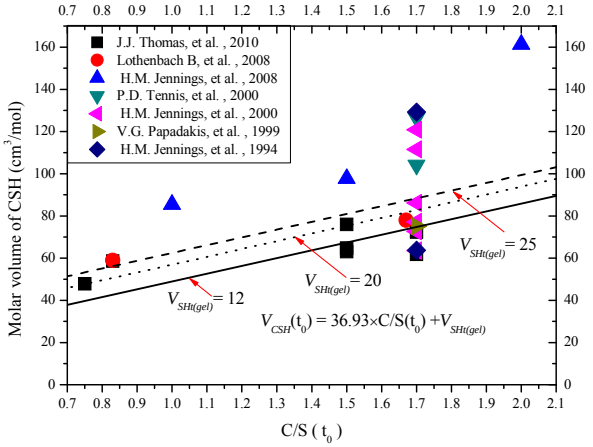

Figure 9 Relations between molar volume and Ca / Si ratio of the C-S-H

From Figure 9, carbonation of most of the species of C-S-H will result in the increase of the porosity of cement paste. It should be noticed that the effects of the carbonation on the porosity evolution will be different for some types of C-S-H, if the value of $V_{SH_i(gel)}$ is chosen as a different value.

Calculated on the basis of the TGA test results, the amounts of calcium carbonate contributed by the carbonation of portlandite or C-S-H were calculated and shown in Figure 10a. Apparently, the proportion of $CaCO_3$ contributed by the carbonation of C-S-H is significantly higher and dominant in the three mixtures blended with a high amount of SCMs such as B70, F10B54 and F30B30. Concerning the cement- fly ash binary system, the same result may be found if the replacement level of FA increases higher than 40%(Thiéry, Faure et al. 2011).

As being discussed, the carbonation of C-S-H contributes an increase of the porosity of carbonated cement paste. And most of the $CaCO_3$ are formed from the carbonation of C-S-H in blended cement paste. Therefore, the carbonation of C-S-H has a dominant effect on the evolution of total porosity in cement paste blended with the high amount of SCMs. Combined with the total porosity tested by MIP, the relationship between the changes of total porosity in cement paste and the amount of C-S-H being carbonated are drawn and illustrated in Figure 10b.

Total porosities of B70 and F10B54 increase with the increasing amount of C-S-H involving in the carbonation; total porosities of P100 and F30 decrease with the increase of the amount of carbonated C-S-H. The total porosity of F30B30 increases after carbonation, however the increment in porosity decreases when the amount of C-S-H being carbonated increases.

In blended cement paste, a large part of C-S-H is produced by the pozzolanic reaction between portlandite and SCMs, defined as low Ca C-S-H in the introduction. The carbonation of the low Ca C-S-H may produce a poorly-hydrated silica gel of a low molar volume due certainly to a release of a great amount of free water initially chemically-bound within the C-S-H during carbonation. This peculiar behavior observed for the pozzolanic C-S-H is more evident with a higher replacement ratio of SCMs (FA> 40% or BFS > 55%) since given that it is observed in Figure 8 and the literature that carbonation can then significantly contribute to an increase in porosity.

It should be noticed that the property of low Ca C-S-H in FA blended cement paste is quite different from that produced from the pozzolanic reaction of BFS. They may have the opposite effects on the porosity development in blended cement paste, see in Figure 10b. The combined effect from the carbonation of these two types of C-S-H results in the particular development of the total porosity in F30B30.

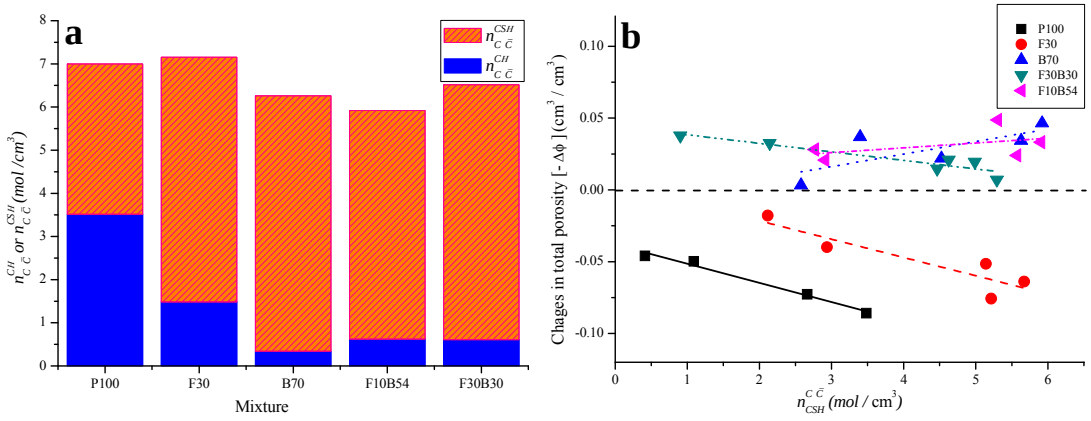

Figure 10 (a) Amounts of $CaCO_3$ contributed by the carbonation of CH ($n_{C\bar{C}}^{CH}$) or CSH ($n_{C\bar{C}}^{CSH}$) (Hydrated for 1 year, then carbonated for 84 days; the surface part). (b) Relationship between the changes of total porosity in cement paste and the amount of C-S-H being carbonated during carbonation

3.2 Effects of carbonation on the gel pore-Nitrogen adsorption test

By using BJH method, the pore size distributions in the range of 2-37 nm are calculated from the nitrogen adsorption test results, as shown in Figure 11. As mentioned in Jennings 'work, the low density (LD) C-S-H structure has a significant amount of internal porosity accessible to the nitrogen, while the high density (HD) C-S-H does not. Therefore, the pores in this scale mainly belong to the gel pores of LD C-S-H, which are divided into two categories: small gel pores (SGP = 1-3 nm) and larger gel pores (LGP = 3-12nm), according to the colloid C-S-H model(Jennings 2008). The intraglobule pores (IGP, ≤ 1nm) is not discussed here because the nitrogen cannot penetrate the intraglobule pores inside the LD C-S-H structure although it is small enough to do so.

Apparently, the pore volume in the range from 2-37 nm declines after carbonation. In the differential curves, the 'critical peak' at around 5 nm appears for virgin sample, but the 'critical peak' at around 22-30 nm disappears for the same sample after carbonation. The first peak indicates the small gel pores and the second peak corresponds to the small capillary pores between the globule flocs which have a size of 30-60nm.

The carbonation of C-S-H is a complex process involving both the decalcification and polymerization of silicate chain. The reconstruction and readjustment in three dimensions will result in the overlaps between silicate chains from the adjacent globules, which creates more small gel pores and increase the size of the 'new' globule. Therefore, the number and the radius of pores between globules increases and contributes to the appearance of the first 'critical peak'. Meanwhile, the polymerization of silicate chain can also causes the shrinkage of C-S-H and the decrease of the size of the 'globule floc'. This will increase the pore size of small capillary pores. Therefore, the 'critical peak' at around 22-30 nm disappears and moves to the capillary pore area with a larger size. This is confirmed by the MIP test results. Evolution of the gel pore structure of C-S-H is described by the schematic diagram shown in Figure 12. This peculiar phenomenon observed indicating the carbonation of C-S-H, especially the low Ca C-S-H is more evident for the mixture with a higher replacement ratio of SCMs, like B70 and F30B30.

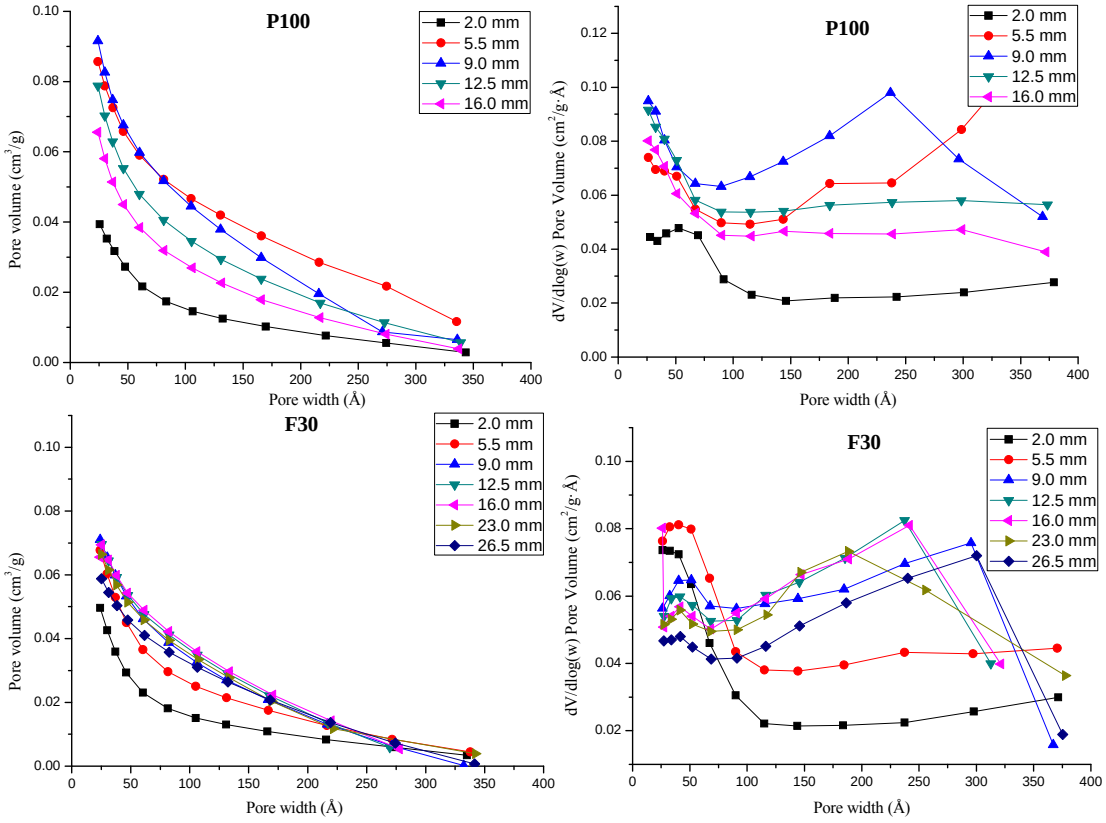

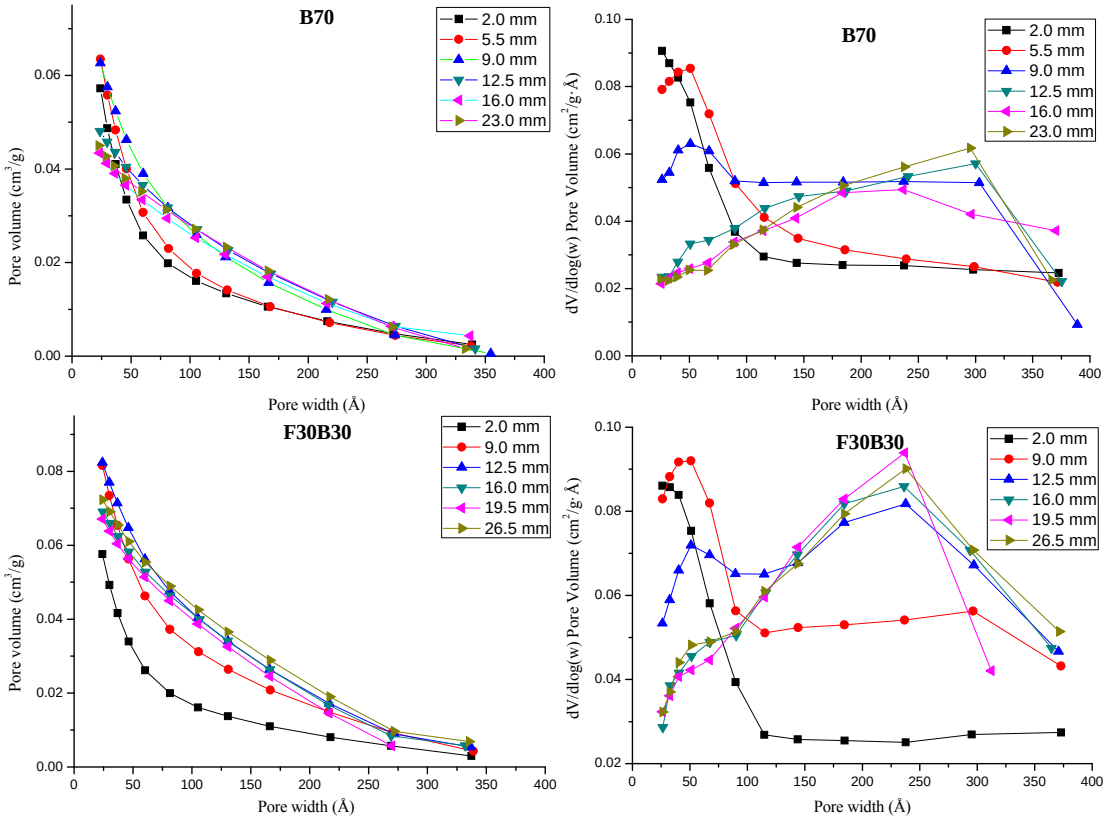

Figure 11 Evolution of accumulative pore volume and pore size distributions (2-37 nm) of different mixture measured by Nitrogen adsorption. (Hydrated for 1 year, then carbonated for 84 days).

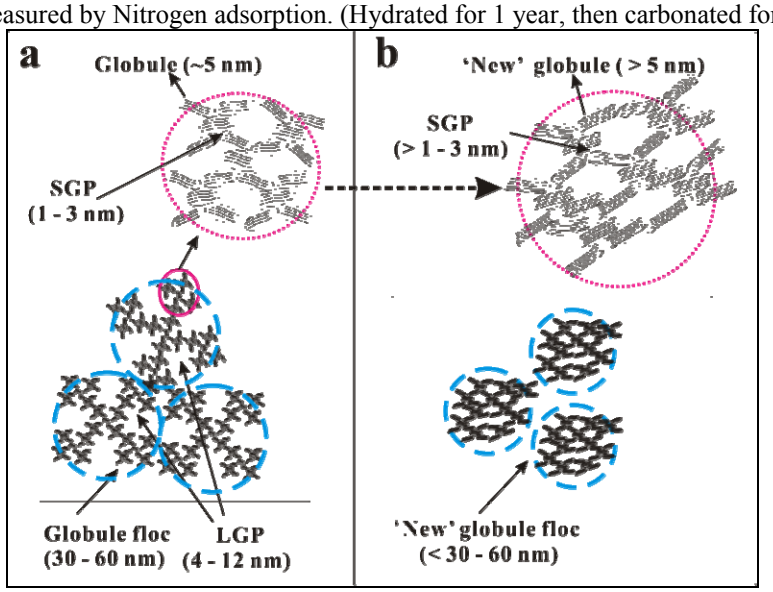

Figure 12 Evolution of the gel pore structure of C-S-H based on the Colloid model: (a) before carbonation; (b) after carbonation.

4. Conclusions

In the paper, the carbonation induced microstructure change in cement paste blended with SCMs is studied by using TGA, MIP and nitrogen adsorption. The evolution of the capillary pore, gel pore structure caused by the carbonation of C-S-H are discussed. The main conclusions are as follow:

- Carbonation can affect the region which is much deeper than the carbonated area determined by the phenolphthalein, especially in blended cement paste. The amount profiles of portlandite and calcium carbonate, determined by TGA test results, can be used as a more accurate method to study the carbonation evolution in cement paste blended with SCMs.

- Carbonation of most of the species of C-S-H results in the increase of the porosity of cement paste.
- The carbonates due to the carbonation of low Ca C-S-H is dominant in blended cement paste B70, F10B54 and F30B30. Both the total porosity and effective capillary porosity increases in the above-mentioned cement paste after carbonation.
- Total porosities of B70 and F10B54 increase with the increasing amount of C-S-H involving in the carbonation. The total porosity of F30B30 increases after carbonation, however, the increment decreases with the increasing amount of C-S-H being carbonated.
- The carbonation of C-S-H increases the volume and size of pores with the radii closer to the small gel pore, and creates more capillary pores. This peculiar phenomenon observed from nitrogen adsorption test is more evident for the mixture with a higher replacement ratio of SCMs, like B70 and F30B30.

Acknowledgements
The authors are grateful for the help from technicians, John van den Berg, Gerrit Nagtegaal Ron Penners and Arjan Thijssen （in alphabetical order of the first letter of their surname） and experimental supports from Microlab, Delft University of Technology. The authors also would like to thank the National Basic Research Program of China (973 Program: 2011CB013800) and the China Scholarship Council (CSC) for the financial support.

References
Auroy, M., S. Poyet, P. Le Bescop, J.-M. Torrenti, T. Charpentier, M. Moskura and X. Bourbon (2015). "Impact of carbonation on unsaturated water transport properties of cement-based materials." Cement and Concrete Research **74**(0): 44-58.
Baird, T., A. G. Cairns-Smith and D. S. Snell (1975). "Morphology and CO2 uptake in tobermorite gel." Journal of Colloid And Interface Science **50**(2): 387-391.
Black, L., C. Breen, J. Yarwood, K. Garbev, P. Stemmermann and B. Gasharova (2007). "Structural features of C–S–H (I) and its carbonation in air—a Raman spectroscopic study. Part II: carbonated phases." Journal of the American Ceramic Society **90**(3): 908-917.
Borges, P. H. R., J. O. Costa, N. B. Milestone, C. J. Lynsdale and R. E. Streatfield (2010). "Carbonation of CH and C–S–H in composite cement pastes containing high amounts of BFS." Cement and Concrete Research **40**(2): 284-292.
Brečević, L. and A. E. Nielsen (1989). "Solubility of amorphous calcium carbonate." Journal of Crystal Growth **98**(3): 504-510.
Chaussadent, T., V. Baroghel-Bouny, H. Hornain, N. Rafaï and A. Ammouche (2000). "Effect of water-cement ratio of cement pastes on microstructural characteristics related to carbonation process." ACI Special Publication **192**.
Chen, J. J., J. J. Thomas and H. M. Jennings (2006). "Decalcification shrinkage of cement paste." Cement and Concrete Research **36**(5): 801-809.
Cole, W. and B. Kroone (1960). Carbon dioxide in hydrated Portland cement. ACI Journal Proceedings, ACI.
Cong, X. D. and R. J. Kirkpatrick (1996). "O-17 MAS NMR investigation of the structure of calcium silicate hydrate gel." Journal of the American Ceramic Society **79**(6): 1585-1592.
Cong, X. D. and R. J. Kirkpatrick (1996). "Si-29 MAS NMR study of the structure of calcium silicate hydrate." Advanced Cement Based Materials **3**(3-4): 144-156.
Cook, R. A. and K. C. Hover (1999). "Mercury porosimetry of hardened cement pastes." Cement and Concrete Research **29**(6): 933-943.

Delmi, M. M. Y., A. Aı¨t-Mokhtar and O. Amiri (2006). "Modelling the coupled evolution of hydration and porosity of cement-based materials." Construction and Building Materials **20**(7): 504-514.
Frías, M. and S. Goñi (2013). "Accelerated carbonation effect on behaviour of ternary Portland cements." Composites Part B: Engineering **48**(0): 122-128.
Glasser, F. and T. Matschei (2007). Interactions between Portland cement and carbon dioxide. Proceedings of the ICCC Conference.
Grattan-Bellew, P. (1996). "Microstructural investigation of deteriorated Portland cement concretes." Construction and Building Materials **10**(1): 3-16.
Jennings, H. M. (2000). "A model for the microstructure of calcium silicate hydrate in cement paste." Cement and Concrete Research **30**(1): 101-116.
Jennings, H. M. (2004). "Colloid model of C−S−H and implications to the problem of creep and shrinkage." Materials and Structures **37**(1): 59-70.
Jennings, H. M. (2008). "Refinements to colloid model of CSH in cement: CM-II." Cement and Concrete Research **38**(3): 275-289.
Jennings, H. M., J. W. Bullard, J. J. Thomas, J. E. Andrade, J. J. Chen and G. W. Scherer (2008). "Characterization and modeling of pores and surfaces in cement paste: correlations to processing and properties." Journal of Advanced Concrete Technology **6**(1): 5-29.
Jennings, H. M. and P. D. Tennis (1994). "Model for the Developing Microstructure in Portland Cement Pastes." Journal of the American Ceramic Society **77**(12): 3161-3172.
Joyner, L. G., E. P. Barrett and R. Skold (1951). "The determination of pore volume and area distributions in porous substances. II. Comparison between nitrogen isotherm and mercury porosimeter methods." Journal of the American Chemical Society **73**(7): 3155-3158.
Lawrence, R. M., T. J. Mays, S. P. Rigby, P. Walker and D. D'Ayala (2007). "Effects of carbonation on the pore structure of non-hydraulic lime mortars." Cement and concrete research **37**(7): 1059-1069.
Litvan, G. G. and A. Meyer (1986). "Carbonation of granulated blast furnace slag cement concrete during twenty years of field exposure." ACI SP **91**(2): 1445-1462.
Lothenbach, B., G. Le Saout, E. Gallucci and K. Scrivener (2008). "Influence of limestone on the hydration of Portland cements." Cement and Concrete Research **38**(6): 848-860.
Lothenbach, B., T. Matschei, G. Möschner and F. P. Glasser (2008). "Thermodynamic modelling of the effect of temperature on the hydration and porosity of Portland cement." Cement and Concrete Research **38**(1): 1-18.
Lothenbach, B., K. Scrivener and R. Hooton (2011). "Supplementary cementitious materials." Cement and Concrete Research **41**(12): 1244-1256.
Marsh, B. K. and R. L. Day (1988). "Pozzolanic and cementitious reactions of fly ash in blended cement pastes." Cement and Concrete Research **18**(2): 301-310.
Matsusato, H., K. Ogawa, M. Funato and T. Sato (1992). Studies on the carbonation of hydrated cement and its effect on microstructure and strength. 9th International Congress on the Chemistry of Cement.
Mindess, S., J. F. Young and D. Darwin (1981). "Concrete, Prentice Hall." Englewood Cliffs, NJ: 481.
Moorehead, D. R. (1986). "Cementation by the carbonation of hydrated lime." Cement and Concrete Research **16**(5): 700-708.

Morandeau, A., M. Thiery and P. Dangla (2014). "Investigation of the carbonation mechanism of CH and CSH in terms of kinetics, microstructure changes and moisture properties." Cement and Concrete Research **56**: 153-170.
Morandeau, A., M. Thiéry and P. Dangla (2015). "Impact of accelerated carbonation on OPC cement paste blended with fly ash." Cement and Concrete Research **67**(0): 226-236.
Ngala, V. T. and C. L. Page (1997). "Effects of carbonation on pore structure and diffusional properties of hydrated cement pastes." Cement and Concrete Research **27**(7): 995-1007.
Nonnet, E., N. Lequeux and P. Boch (1999). "Elastic properties of high alumina cement castables from room temperature to 1600 C." Journal of the European Ceramic Society **19**(8): 1575-1583.
Noumowé, A. (1995). Effet des hautes températures (20 °C–600 °C) sur le béton. PhD.
Papadakis, V. G. (1999). "Effect of fly ash on Portland cement systems: Part I. Low-calcium fly ash." Cement and Concrete Research **29**(11): 1727-1736.
Papadakis, V. G., C. G. Vayenas and M. N. Fardis (1991). "Physical and chemical characteristics affecting the durability of concrete." ACI Materials Journal **88**(2).
Patel, R. G., D. C. Killoh, L. J. Parrott and W. A. Gutteridge (1988). "Influence of curing at different relative humidities upon compound reactions and porosity in Portland cement paste." Materials and Structures **21**(3): 192-197.
Peter, M., A. Muntean, S. Meier and M. Böhm (2008). "Competition of several carbonation reactions in concrete: a parametric study." Cement and Concrete Research **38**(12): 1385-1393.
Pihlajavaara, S. E. (1968). "Some results of the effect of carbonation on the porosity and pore size distribution of cement paste." Matériaux et Construction **1**(6): 521-527.
Pihlajavaara, S. E. and E. Pihlman (1974). "Effect of carbonation on microstructural properties of cement stone." Cement and Concrete Research **4**(2): 149-154.
Platret, G. (2002). "Suivi de l'hydratation du ciment et de l'évolution des phases solides dans les bétons par analyse thermique." Caractéristiques microstructurales et propriétés relatives à la durabilité des bétons. Méthodes de mesure et d'essai de laboratoire. Méthodes d'essai(58).
Puertas, F., M. Palacios and T. Vázquez (2006). "Carbonation process of alkali-activated slag mortars." Journal of Materials Science **41**(10): 3071-3082.
Richard, N. (1999). Structure et propriétés élastiques des phases cimentières base de mono-aluminate de calcium.
Richardson, I. (1999). "The nature of CSH in hardened cements." Cement and Concrete Research **29**(8): 1131-1147.
Richardson, I. and G. Groves (1993). "The incorporation of minor and trace elements into calcium silicate hydrate (C S H) gel in hardened cement pastes." Cement and Concrete Research **23**(1): 131-138.
Song, H.-W. and S.-J. Kwon (2007). "Permeability characteristics of carbonated concrete considering capillary pore structure." Cement and Concrete Research **37**(6): 909-915.
Stepkowska, E., M. A. Aviles, J. M. Blanes and J. L. Perez-Rodriguez (2007). "Gradual transformation of Ca(OH)2 into CaCO3 on cement hydration." Journal of Thermal Analysis and Calorimetry **87**(1): 189-198.
Stepkowska, E. T., J. M. Blanes, F. Franco, C. Real and J. L. Pérez-Rodríguez (2004). "Phase transformation on heating of an aged cement paste." Thermochimica Acta **420**(1-2 SPEC. ISS.): 79-87.

Tennis, P. D. and H. M. Jennings (2000). "A model for two types of calcium silicate hydrate in the microstructure of Portland cement pastes." Cement and Concrete Research **30**(6): 855-863.
Thiéry, M., P. Faure, A. Morandeau, G. Platret, J.-F. Bouteloup, P. Dangla and V. Baroghel-Bouny (2011). Effect of carbonation on the microstructure and moisture properties of cement-based materials. XII DBMC (12th International Conference on Building Materials and Components.
Thomas, J. J., H. M. Jennings and A. J. Allen (2010). "Relationships between Composition and Density of Tobermorite, Jennite, and Nanoscale CaO− SiO2− H2O." The Journal of Physical Chemistry C **114**(17): 7594-7601.
Villain, G. and M. Thiery (2005). Impact of carbonation on microstructure and transport properties of concrete. Proceedings of.
Ye, G. (2003). Experimental study and numerical simulation of the development of the microstructure and permeability of cementitious materials, TU Delft, Delft University of Technology.
Ye, G. (2003). "Experimental study and numerical simulation of the development of the microstructure and permeability of cementitious materials."
Zdeneˇk Sˇauman, V. r. L. (1972). "Long-term carbonization of the phases 3CaO.Al2O3.6H2O and 3CaO.Al2O3.SiO2.4H2." Cement and Concrete Research **2**(4): 12.
Zhou, Q. and F. Glasser (2001). "Thermal stability and decomposition mechanisms of ettringite at< 120 C." Cement and Concrete Research **31**(9): 1333-1339.